# Neurons generated by direct conversion of fibroblasts reproduce synaptic phenotype caused by autism-associated neuroligin-3 mutation

Soham Chanda[a,b,c,d], Samuele Marro[c,d], Marius Wernig[c,d,1], and Thomas C. Südhof[a,b,1]

Departments of [a]Molecular and Cellular Physiology and [d]Pathology, [b]Howard Hughes Medical Institute, and [c]Institute for Stem Cell Biology and Regenerative Medicine, Stanford University School of Medicine, Stanford, CA 94305

Contributed by Thomas C. Südhof, August 28, 2013 (sent for review July 30, 2013)

**Recent studies suggest that induced neuronal (iN) cells that are directly transdifferentiated from nonneuronal cells provide a powerful opportunity to examine neuropsychiatric diseases. However, the validity of using this approach to examine disease-specific changes has not been demonstrated. Here, we analyze the phenotypes of iN cells that were derived from murine embryonic fibroblasts cultured from littermate wild-type and mutant mice carrying the autism-associated R704C substitution in neuroligin-3. We show that neuroligin-3 R704C-mutant iN cells exhibit a large and selective decrease in AMPA-type glutamate receptor-mediated synaptic transmission without changes in NMDA-type glutamate receptor- or in $GABA_A$ receptor-mediated synaptic transmission. Thus, the synaptic phenotype observed in R704C-mutant iN cells replicates the previously observed phenotype of R704C-mutant neurons. Our data show that the effect of the R704C mutation is applicable even to neurons transdifferentiated from fibroblasts and constitute a proof-of-concept demonstration that iN cells can be used for cellular disease modeling.**

cellular reprogramming | stem cells | postsynaptic density | neurexin | synapse

In a revolutionary technical achievement during the last decade, induced pluripotent stem (iPS) cells now can be generated from nearly every somatic cell type (1–3). Moreover, efficient protocols now are available to guide the differentiation of iPS cells and embryonic stem (ES) cells into different types of neurons that then can be used for disease modeling (4–7). As a further development, we and others recently described direct conversion of nonneural cells into induced neuronal (iN) cells, which accelerates the generation of neurons from nonneuronal cells and renders this process more uniform and less variable (8–16). The iN cells behave like functional neurons in that they display neuron-like morphologies, express neuronal marker genes, fire action potentials (APs), and, at least in some instances, are not only the postsynaptic recipients of input synapses but also form presynaptic output synapses onto each other or onto cocultured primary neurons.

The in vitro generation of neurons from nonneuronal cells is of great interest because of its potential for studying neural development and for producing neurons for regenerative medicine. A possibly even more important application may be the use of neurons transdifferentiated from nonneuronal cells for examining disease mechanisms, because transdifferentiated neurons can be obtained from living patients. Indeed, a large number of studies reported a multitude of disease-related changes in neurons differentiated from patient-derived iPS cells (17–20), and even iN cells have been used for this purpose (13). However, to date no study has tested whether the neurons directly reprogrammed from fibroblasts, ES cells, or other nonneural cells actually can recapitulate a phenotype observed in primary neurons from the same organism.

To address this important question, we asked whether iN cells derived from a mutant mouse with a defined synaptic phenotype can recapitulate the effect. We focused on a previously characterized autism-associated mutation in neuroligin-3 because of its disease relevance (21, 22). Neuroligins are postsynaptic cell-adhesion molecules that interact with presynaptic neurexins and other ligands (22). Mice and humans express four neuroligin genes. Neuroligin-1 (*Nlgn1*) is specific for excitatory synapses (23), and neuroligin-2 (*Nlgn2*) is specific for inhibitory synapses (24). The localization of neuroligin-3 (*Nlgn3*) and neuroligin-4 (*Nlgn4*) is less clear, but they may be expressed in both types of synapses. All neuroligins exhibit a conserved domain structure containing a large extracellular esterase-homology domain, a single transmembrane region, and a short cytoplasmic tail with a C-terminal PDZ-domain binding sequence (25, 26). Mutations in neuroligins have been associated with autism-spectrum disorders (ASDs) and appear to be nearly 100% penetrant (22, 27).

Among candidate genes for ASDs, neuroligins are particularly interesting because of their role as postsynaptic cell-adhesion molecules and because several of their interacting partners, including neurexins and Shanks, also have been implicated in ASDs (22). To examine the pathogenic mechanism of Nlgn3 mutations in ASDs, we previously produced KO mice that lack *Nlgn3* expression and knockin mice that contain the ASD-associated point mutations R451C or R704C. These mice exhibit major synaptic phenotypes (21, 28, 29). Among neuroligin mutations, the R704C mutation (which affects a conserved arginine residue on the cytoplasmic face of the transmembrane region) was arguably the most interesting, in that it produced a selective decrease in AMPA-type glutamate receptor (AMPAR)-mediated responses

## Significance

**A major challenge in modeling human diseases is to replicate disease phenotypes in neurons that are differentiated from nonneuronal cells, such as pluripotent stem cells or fibroblasts. However, evidence that phenotypes observed with this approach replicate an endogenous disease phenotype is lacking. This study demonstrates that induced neuronal (iN) cells obtained by direct conversion of fibroblasts to neurons, when produced from a previously described mouse mutant in neuroligin-3 that is linked to autism, exhibited a phenotype similar to that observed in endogenous neurons. These data show that the mutation studied is highly penetrant phenotypically and also that iN cells can faithfully reproduce a phenotype observed in endogenous neurons, thus validating the use of iN cells for studying disease models.**

Author contributions: S.C., M.W., and T.C.S. designed research; S.C. and S.M. performed research; S.C., S.M., and T.C.S. analyzed data; and M.W. and T.C.S. wrote the paper.

The authors declare no conflict of interest.

[1]To whom correspondence may be addressed. E-mail: wernig@stanford.edu or tcs1@stanford.edu.

This article contains supporting information online at www.pnas.org/lookup/suppl/doi:10.1073/pnas.1316240110/-/DCSupplemental.

at excitatory synapses; however, the cellular basis of this phenotype remains unclear (21).

Here, we asked whether the phenotype produced by the *Nlgn3* R704C mutation can be equally found in iN cells obtained from these mice. To address this question, we explored the phenotype of mutant and WT iN cells obtained from littermate mice. Our data reveal that the R704C mutation produces a loss of cell-surface AMPARs but not NMDA receptors (NMDARs), resulting in a dramatic decrease in excitatory synaptic strength and a shift in the excitatory/inhibitory balance, and that the iN cell phenotype is surprisingly similar to that we observed in hippocampal neurons (21). These results validate the overall principal approach of analyzing neurons obtained from nonneuronal cells and confirm the utility of iN cells for analyzing disease mechanisms.

## Results

***Nlgn3* R704C Mutation Does Not Impact iN-Cell Reprogramming or iN-Cell Intrinsic Membrane Properties.** To examine whether the synaptic phenotype of R704C-mutant neurons observed in primary hippocampal neurons (21) can be reproduced using iN cells that were obtained by transdifferentiation of fibroblasts, we crossed *Nlgn3* R704C-mutant mice with mice expressing EGFP transcribed from the endogenous *tau* gene locus (30). Because tau expression is neuron specific, EGFP expression in cells derived from these mice allows direct monitoring of iN cell generation. We then cultured mouse embryonic fibroblasts (MEFs) from littermate WT and R704C-mutant mice that also contained the EGFP-tau insertion and converted the MEFs into iN cells by transduction of three transcription factors (Brn2, Ascl1, and Myt1L; BAM) as described (Fig. 1*A*) (8). Two weeks after expression of the transcription factors, the resulting iN cells displayed a typical neuronal morphology (Fig. 1*B*). We found a similarly strong induction of Nlgn3 mRNA expression in WT and R704C-mutant iN cells as measured by quantitative RT-PCR, with levels that were approximately half of those observed in adult mouse brain (Fig. 1*C*). We detected no significant difference between WT and R704C-mutant MEFs in the efficiency of iN cell conversion as quantified as the fraction of cells that activate the TAU::EGFP reporter (Fig. 1*D*).

Motivated by these findings, we set out to compare the synaptic properties of WT and R704C-mutant iN cells. Because iN cells derived with the BAM transcription factors from MEFs are mostly excitatory (8), and a pure culture of iN cells would restrict our study to excitatory AMPAR- and NMDAR-mediated synaptic responses, we cocultured iN cells that express EGFP with primary neurons cultured from a WT mouse that does not express EGFP. We purified tau-EGFP–positive iN cells by FACS 6 d postinduction and plated them on top of primary olfactory bulb neurons derived from WT mice. The iN cells were cocultured with the olfactory bulb neurons for an additional 16–18 d after cell sorting (Fig. 1 *E* and *F* and Fig. S1). As shown previously, iN cells that are cocultured with primary neurons become the postsynaptic recipient of both excitatory and inhibitory synapses derived from the primary neurons, in addition to forming presynaptic specializations with each other and with the primary neurons (8, 16). This circumstance may be particularly useful in our case, because Nlgn3 is a postsynaptic cell-adhesion protein, suggesting that its role in synaptic transmission should be preserved in postsynaptic tau-EGFP–positive iN cells obtained from WT or R704C-mutant mice.

We performed whole-cell current-clamp recordings from tau-EGFP–positive iN cells (Fig. S1). We found that these cells express voltage-gated $Na^+$ and $K^+$ channels and receive both excitatory (AMPAR- and NMDAR-mediated) and inhibitory GABA receptor (GABAR)-mediated synaptic connections from neighboring neurons (Fig. 2 and Fig. S2). This result suggests that the iN cells are similar to primary neurons in terms of intrinsic and synaptic properties (Figs. 2 and Fig. S2). We measured

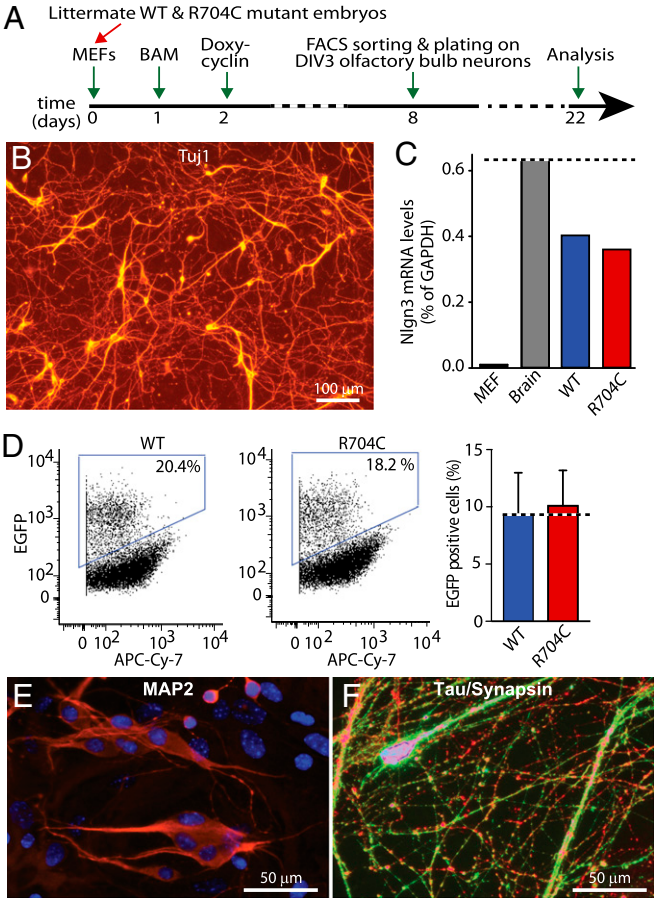


**Fig. 1.** Generation of iN cells from MEFs isolated from WT and *Nlgn3* R704C-mutant mice. (*A*) Schematic representation of the experimental design. MEFs were seeded on day 0 and transduced with the BAM transcription factors on day 1, and transgene expression was induced by the addition of doxycycline to the medium on day 2. Olfactory bulb neurons were cultured from newborn WT mice on day 5, tau-EGFP–positive iN cells were isolated by FACS sorting and placed on top of the primary neurons on day 6, and electrophysiological and imaging experiments were performed on days 22–24. (*B*) Representative image of R704C-mutant iN cells stained 14 d after transduction of MEFs for the pan-neuronal marker Tuj1. (*C*) Representative quantitative RT-PCR analysis of *Nlgn3* expression in MEFs, mouse brain, and WT and R704C-mutant iN cells that were analyzed without FACS sorting 20 d posttransduction. (*D*) (*Left*) FACS analysis illustrating the efficiency of the conversion of MEFs into iN cells (defined as tau-EGFP–positive cells) in R704C-mutant and WT cells. (*Right*) The bar graph shows the average abundance of tau-EGFP–positive cells ($n = 5$ experiments). (*E* and *F*) Immunofluorescence analysis of iN cells (cultured on glia only). At day 20, iN cells were stained for DAPI (blue) and MAP2 (red) (*E*) and for tau-GFP (green), synapsin (red), and DAPI (blue) (*F*).

the AP firing parameters of WT and R704C-mutant iN cells by applying step current pulses of increasing amplitude (Fig. 2 *A* and *B*). Both types of iN cells fired single or multiple APs upon current injections (Fig. 2*A*) and displayed mature membrane properties (Fig. 2*B*) with no detectable difference in AP firing properties between WT and R704C-mutant iN cells (Fig. 2 *A* and *B* and Fig. S3). Furthermore, when we measured $Na^+$ and $K^+$ currents from WT and R704C-mutant iN cells, we found no significant change (Figs. 2*C*). Also, the membrane capacitance and input resistance were not significantly different in WT and R704C-mutant iN cells (Fig. 2 *D* and *E*). These data indicate that iN cells derived from WT and R704C-mutant mouse fibroblasts are similarly mature and that the R704C mutation in *Nlgn3* does not detectably affect the reprogramming process or cell-intrinsic properties

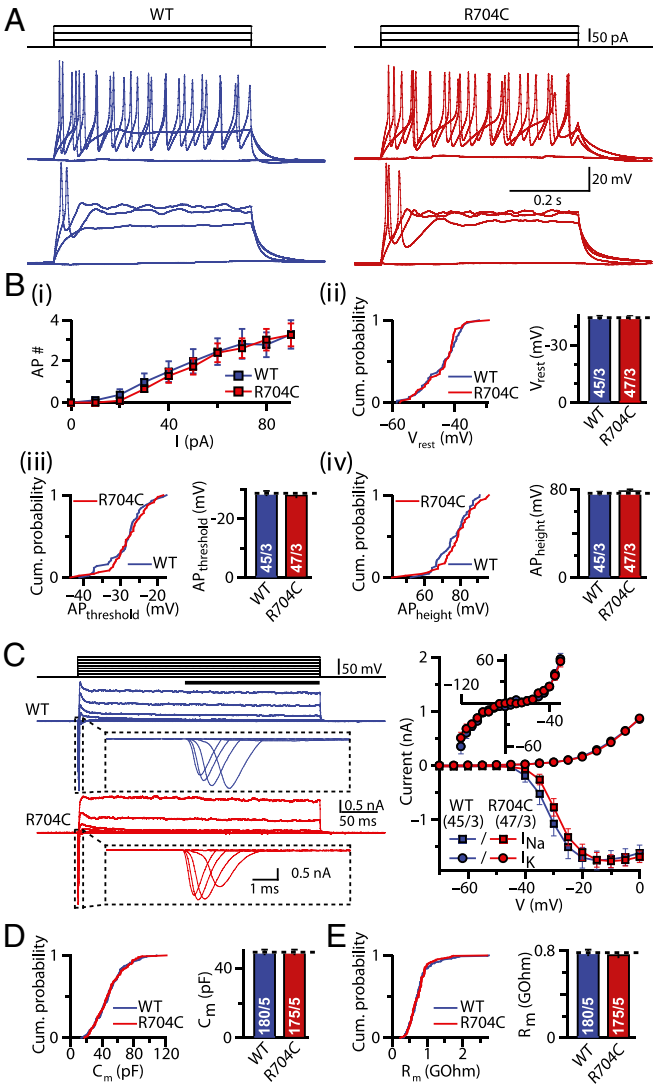


**Fig. 2.** iN cells derived from WT and *Nlgn3* R704C-mutant mice have similar intrinsic electrical properties. (*A* and *B*) Analysis of AP firing properties in WT (blue) and R704C-mutant iN cells (red). iN cells were patched in current-clamp mode and injected with current pulses increasing in 10-pA increments. (*A*) Experimental protocol (*Top*) and representative traces of AP firing patterns consisting of multiple (*Middle*) or single (*Bottom*) APs. (*B*) Quantitative analyses of (*i*) the number of APs induced by a current pulse, (*ii*) the resting membrane potential, (*iii*) the AP firing threshold, and (*iv*) the AP amplitude. No statistically significant difference ($P > 0.5$) between WT and R704C-mutant iN cells was detected in any parameter. In all subpanels, the number of cells/cultures analyzed is indicated in the corresponding bar graphs. (*C*) Analysis of $Na^+$ and $K^+$ currents in WT (blue) and R704C-mutant (red) iN cells. (*Left*) The experimental voltage pulse step protocol (black, *Top*), and examples voltage-clamp recording traces ($V_{hold} = -70$ mV). Expanded views of $Na^+$ currents are shown in the dashed boxes below the traces. The black line below the protocol diagram depicts the time period used for calculating average $K^+$ currents. (*Right*) The average $Na^+$ currents ($I_{Na}$, filled squares) and $K^+$ currents ($I_K$, filled circles) recorded from WT and R704C-mutant iN cells and plotted as a function of the step-voltage amplitudes. (*Inset*) The reversal potential ($V_{rev}$) for $K^+$ currents. No significant difference was found between WT and R70C-mutant iN cells at any step size tested ($P > 0.2$, unpaired, one-tailed *t* test). (*D* and *E*) Analysis of the capacitance (*D*) and input resistance (*E*) of WT (blue) and R704C-mutant iN cells (red). No significant difference was found for either parameter ($P > 0.8$, *t* test).

of iN cells. They also suggest that fibroblast-derived iN cells have a high degree of reproducibility.

**Selective Synaptic Defect in R704C-Mutant iN Cells.** We next sought to characterize the synaptic properties of WT and R704C-mutant iN cells. MEF iN cells derived from WT and R704C-mutant animals exhibited a similar distribution of cells with or without measurable synaptic responses (Fig. S3), suggesting that WT and R704C-mutant iN cells form synaptic connections with neighboring neurons with a similar efficiency (~70%). To be careful, we subsequently included in our comparative analysis of WT and R704C-mutant neurons only iN cells with detectable synaptic responses.

We first measured AMPAR-driven miniature excitatory postsynaptic currents (mEPSCs) from WT and R704C-mutant iN cells in the presence of the voltage-gated $Na^+$-channel inhibitor tetrodotoxin (TTX) to block AP-triggered synaptic transmission in the cultures. We found a significant decrease in mEPSC amplitude and frequency in R704C-mutant iN cells (Fig. 3*A*). The decrease was particularly dramatic for the mEPSC frequency, which was depressed by >50%. We also measured AMPAR-mediated spontaneous EPSCs and GABAR-mediated spontaneous inhibitory postsynaptic currents (IPSCs) from iN cells in the presence of the $GABA_A$-receptor blocker picrotoxin or the AMPAR blocker 6-cyano-7-nitroquinoxaline-2,3-dione (CNQX), respectively. We found a significant decrease in the frequency of spontaneous EPSCs but not in their amplitude (Fig. 3*B*), consistent with a decrease in functional AMPAR-containing synapses as suggested by the decrease in mEPSC frequency. In contrast, we found no changes in the frequency or amplitude of spontaneous IPSCs (Fig. 3*C*). Overall, these data suggest that the *Nlgn3* R704C mutation specifically reduces AMPAR-mediated synaptic transmission in fibroblast-derived iN cells, similar to its effect on hippocampal neurons (21).

To test this hypothesis further, we directly measured AMPAR-mediated evoked EPSCs in WT and R704C-mutant iN cells. Again, R704C-mutant iN cells exhibited a significant decrease in EPSC amplitude compared with WT iN cells (Fig. 4*A*). To probe whether this decrease in AMPAR-mediated EPSCs is caused by a presynaptic change in release probability, we calculated the coefficient of variation of evoked EPSCs but found no significant difference between WT and R704C-mutant conditions (Fig. 4*A*, *Lower Right*). This result supports the notion based on the localization of *Nlgn3* that the decrease in AMPAR-mediated synaptic transmission in R704C-mutant iN cells is caused by a postsynaptic mechanism.

In contrast to its effect on AMPAR-mediated EPSCs, the R704C mutation did not alter NMDAR-mediated EPSCs (Fig. 4*B*). Moreover, paired-pulse ratio (PPR) measurements of NMDAR-mediated EPSCs also detected no difference between WT and R704C-mutant iN cells (Fig. 4*C*), further strengthening the evidence that presynaptic glutamate release was not altered significantly by the R704C mutation. Note that such PPR measurements cannot be performed for AMPAR-mediated EPSCs in a straightforward manner in cultured neurons because in most trials AMPAR-driven network activity after the first evoked response makes it difficult to quantify the second EPSC of a paired-pulse (for example, see Fig. S2*B*). Similarly, IPSCs were unchanged by the R704C mutation (Figs. 4 *D* and *E*).

To assess if the R704C mutation in *Nlgn3* affects AMPAR gating, we analyzed the kinetics of mEPSCs from WT and R704C-mutant iN cells; we found no significant difference between two types of iN cells (Fig. S4), suggesting that the physical properties of AMPARs were unaffected. In a final experiment, we puffed AMPA directly onto WT and R704C-mutant iN cells to estimate their relative surface levels of AMPARs. We found a significant decrease in the peak amplitude and the total charge transfer of the AMPA-puff response in R704C-mutant iN cells compared with WT iN cells (Fig. 4*F*), corroborating the conclusion that R704C-mutant iN cells contain a lower concentration of surface AMPARs.

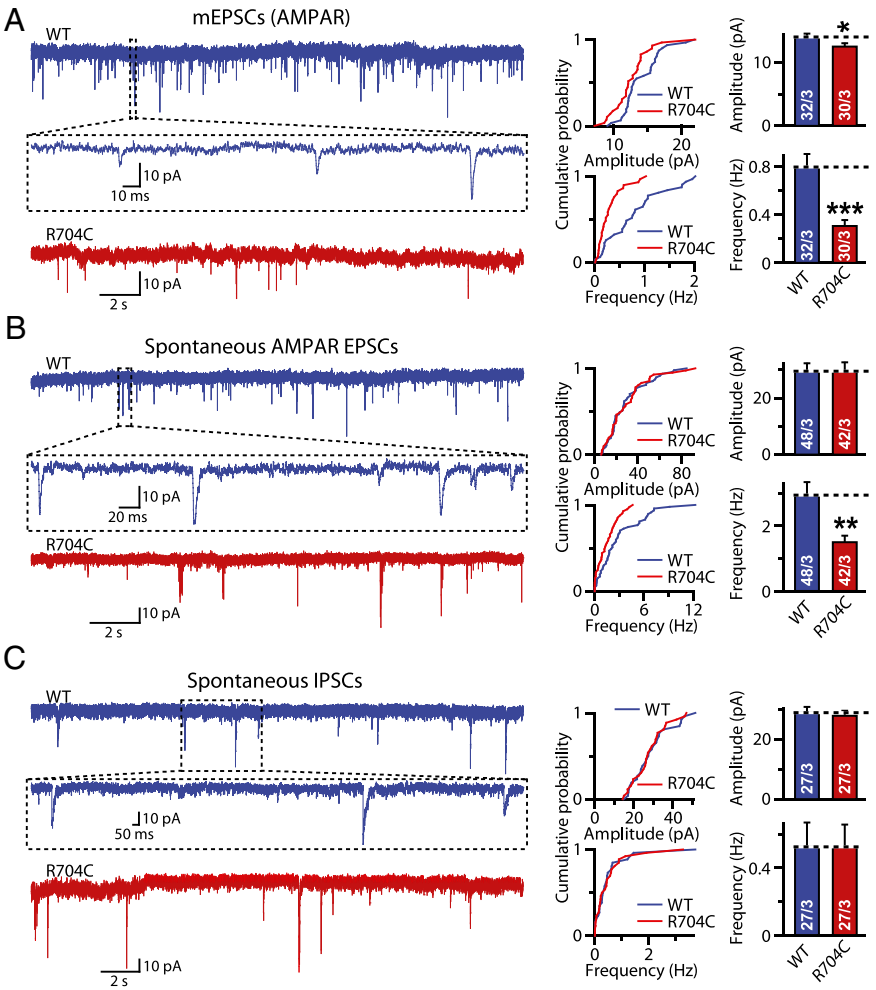


**Fig. 3.** iN cells derived from *Nlgn3* R704C-mutant mice show significant decreases in AMPAR-mediated synaptic transmission. (*A*) Analysis of spontaneous mEPSCs. (*Left*) Sample traces.The dashed box depicts an expanded trace to illustrate the EPSC kinetics. (*Right*) Cumulative probability plots and bar graphs of the mEPSC amplitude (*Upper*) and frequency (*Lower*). mEPSCs were recorded from WT (blue) and R704C-mutant iN (red) cells in 50 μM picrotoxin and 1 μM TTX. (*B*) Spontaneous EPSCs measured in WT (blue) and R704C-mutant iN (red) cells in 50 μM picrotoxin and 50 μM AP5. Data are presented as in *A*. (*C*) As in *B*, except that spontaneous IPSCs were examined in the presence of 50 μM CNQX. Data shown in the bar diagrams are means ± SEM; number of cells/independent cultures analyzed are indicated in the bars. Statistical significance levels were assessed by unpaired, one-tailed Student *t* test (**P* < 0.05, ***P* < 0.01, and ****P* < 0.001, all versus control).

## Discussion

Despite a large number of studies examining the phenotype of neurons differentiated from patient-derived iPS cells (13, 17–20), the effect of an identified mutation on synaptic transmission has not been compared between a native neuron and a neuron differentiated from a nonneuronal cell. This gap in our knowledge may be particularly pressing for iN cells, because the derivation of iN cells from nonneuronal cells in a single step by forced expression of transcription factors may be considered to be more artificial than differentiating ES or iPS cells into neurons. However, even neurons differentiated from iPS or ES cells are obtained by complex protocols that only distantly mimic physiological conditions and do not necessarily represent native differentiation states. Furthermore, protocols for neuronal differentiation from iPS or ES cells often are tedious and require multiple rounds of patterning factor treatments. On the other hand, direct transdifferentiation of nonneuronal cells into iN cells generally is faster, is highly reproducible, and exhibits higher conversion efficiency (16). To test whether neurons produced by direct reprogramming of fibroblasts also can be used to model disease states induced by a genetic mutation, we here analyze MEF iN cells derived from littermate WT and *Nlgn3* R704C-mutant mice. We demonstrate that, at least for the R704C mutation studied here, which was chosen because of its discrete and robust phenotype (21), iN cells accurately replicate the synaptic phenotype of endogenous neurons.

Thus, although iN cells are likely not as mature as primary neurons, they exhibit quantitative and reproducible neuron-specific traits that recapitulate the properties of native neurons and can be used to phenotype the effects of a specific mutation. This finding sets the stage for using iN cells for phenotyping not only mutant mouse neurons but also human neurons. We previously have reported that iN cells can be generated rapidly and with high efficiency from human fibroblasts and ES/iPS cells (9, 16). The present finding obtained with R704C-mutant mouse fibroblasts provides a starting platform for performing comparable synaptic studies on human fibroblasts or iPS cells derived from patients or on mutant human cells in which a particular defined gene mutation has been introduced. Although difficult, such studies might provide insight into the pathophysiology of a disease-associated mutation in human patients and possibly might lead to the development of therapeutic approaches (31).

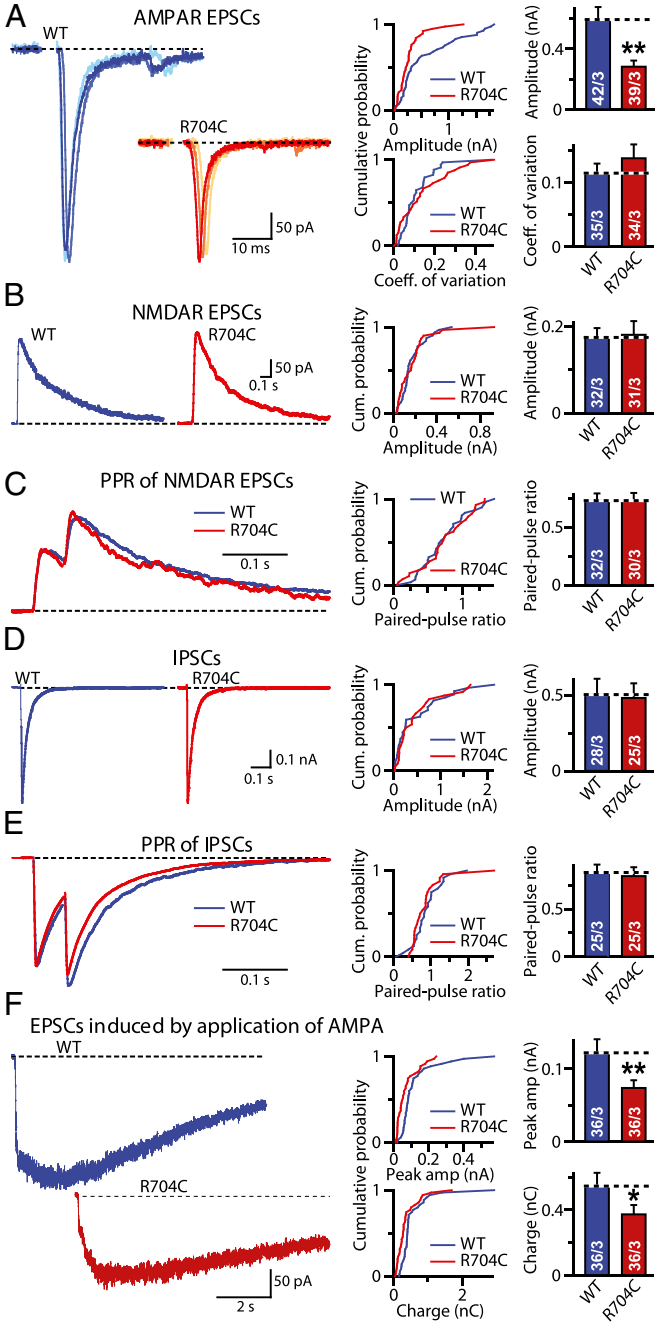


**Fig. 4.** R704C-mutant iN cells exhibit reduced evoked AMPAR- but not GABAR-mediated synaptic responses. (*A*) Analysis of evoked AMPAR-mediated EPSCs in WT (blue) and R704C-mutant iN (red) cells. EPSCs were evoked by extracellular stimulation in the presence of 50 μM picrotoxin and 50 μM AP5. (*Left*) Example traces show three consecutive trials for each example (shades) that are overlaid with a small lateral shift for better visibility. (*Center*) Cumulative probability plots depict the EPSC amplitude (*Upper Center*) and coefficient of variation as a measure of release probability (*Lower Center*). (*Right*) Bar graphs display the means ± SEM of the respective parameters. (*B*) As in *A*, but for NMDAR-mediated EPSCs without analysis of the coefficient of variation. Traces depict only a single example. (*C*) Analysis of PPRs (interstimulus interval, 50 ms) to assess the release probability. (*Left*) Scaled sample traces. (*Center*) Cumulative probability plots of PPRs. (*Right*) Mean PPR. (*D*) As in *B*, but for IPSCs. (*E*) As in *C*, but for IPSCs. (*F*) Analysis of EPSCs induced by direct application of AMPA (50 μM) in WT (blue) and R704C-mutant iN (red).cells. (*Left*) Representative traces. (Center) Cumulative probability plots of the EPSC amplitude (*Upper*) and charge transfer (*Lower*). (*Right*) Bar graphs of the mean values for the same parameters. Data shown in the bar graphs are means ± SEM; numbers of cells/independent cultures analyzed are stated in the bars. $^{*}P < 0.05$; $^{**}P < 0.01$, Student *t* test.

In particular, the value of the mutagenesis approach lies in the possibility of performing the accordant analyses with tight controls that rule out changes induced by clonal variation and differences in genetic background. Such changes otherwise might introduce a significant degree of variability into the analyses and cannot be easily controlled for by comparing neurons differentiated from iPS cells.

In addition to validating iN cells as a model system, our study provides insights into the function of *Nlgn3* and its relation to AMPARs. Our data show that the R704C mutation decreases not only the mEPSC frequency but also the mEPSC amplitude. The data thus suggest that the R704C mutation may selectively decrease the concentration of postsynaptic AMPARs. The decreases in mEPSC frequency and in the frequency of spontaneous events in iN cells produced by the R704C mutation likely reflect a relative increase in silent or nearly silent synapses that are undetectable during these measurements. Among others, our results corroborate the notion that Nlgn3 is not simply a postsynaptic cell-adhesion molecule involved in establishing synaptic connections but that it contributes to determining the properties of synapses, e.g., in the present case, the relative content of AMPARs at a given synapse. The effect of the *Nlgn3* R704C-mutation on AMPAR responses is surprisingly strong (~50% decrease) given the continued presence of other neuroligins that might be redundant. Moreover, no similar effect was observed in *Nlgn3* KO neurons (28, 29). Together, these observations indicate that the R704C mutation does not operate as a loss-of-function mutation in which AMPARs are insufficiently retained on the neuronal surface but rather as a gain-of-function mutation in which the single amino acid substitution of the R704C mutation induces the removal of AMPARs from the surfaces. Considering the robustness of the effect, it would be extremely interesting to study potential mechanisms of this phenotype in future studies.

## Experimental Procedures

**Cell Culture.** MEFs were established from embryonic day 13.5 embryos, as described (8). At passage three, 250,000 cells were plated on an uncoated 3-cm polystyrene dish (BD Falcon) and were transduced on the next day using doxycycline-inducible TetO-FUW–based lentivirus containing the cDNAs for Ascl1-T2A-Brn2, Myt1l, and rtTA. Doxycycline was added the day after viral infection, and the medium was changed to N3 [DMEM/F12 (Life Technologies), and 25 μg/mL insulin, 50 μg/mL apo-transferrin, 30 nM sodium selenite, 20 nM progesterone, 100 nM putrescine (Sigma)] on the following day.

**Quantitative PCR.** Total RNA was isolated from non–FAC-sorted pure MEF-iN cultures (without any coculture) 20 d after transduction (day 22) using the RNeasy kit according to the manufacturer's instruction (Qiagen). Total RNA (0.5 μg) was reverse-transcribed using the SuperScript First-Strand Synthesis System (Invitrogen). Quantitative RT-PCR was performed using the 7900HT Real-Time PCR System (Applied Biosystems) and TaqMan Gene Expression Assays for GAPDH (Mm99999915_g1) and Nlgn3 (87830249 -customized assay). Expression values were expressed as percent GAPDH using the formula: $2^{-CT\ NLGN3}/2^{-CT\ GAPDH} \times 100$.

**Immunofluorescence, RT–PCR, and Flow Cytometry.** Neuronal cells were defined as cells that stained positive for Tuj1 and had neurites at least three times longer than the cell body. Immunofluorescence staining was performed as described (8). EGFP-expressing cells were analyzed and sorted on a FACS Aria II, and flow cytometry data were analyzed using FACS Diva Software (Becton Dickinson). The following antibodies were used for analyses: mouse anti-MAP2 (Sigma, 1:500), mouse anti-NeuN (1:100; Millipore), rabbit anti-Tuj1 (1:1,000; Covance), E028 rabbit anti-synapsin (1:500), guinea-pig anti-vGLUT1 (1:2,000; Millipore) and Alexa-488– and Alexa-555–conjugated secondary antibodies (Invitrogen).

**Mice.** We crossed homozygous tau-EGFP knockin mice (Jackson Laboratory) (30) with WT or *Nlgn3* R704C knockin mice (29) to generate tau-EGFP–positive WT and R704C-mutant mice. Genotyping was performed by PCR using oligonucleotide primers KT06470 and KT06471 as described (29).

**Primary Cultures of Olfactory Bulb Neurons.** Primary cultures of mouse olfactory bulb neurons were obtained essentially as described (32, 33).

**Electrophysiology.** The tau-EGFP–positive iN cells were visualized using an X-cite 120Q fluorescence lamp (Lumen Dynamics) and an Olympus BX51WI microscope equipped with a Rolera-XR camera (Qimaging). Whole-cell patches were established at room temperature using MPC-200 manipulators (Sutter Instrument) and a Multiclamp 700B amplifier (Molecular Devices) controlled by Clampex 10 Data Acquisition Software (Molecular Devices). Pipettes were pulled using a PC-10 puller (Narishige) from borosilicate glass (o.d. 1.5 mm, i.d. 0.86 mm; Sutter Instrument) to a resistance of 2–3 MOhm and were filled with internal solution containing for voltage-clamp (in mM) 135 $CsCl_2$, 10 Hepes, 1 EGTA, 1 Na-GTP, and 1 QX-314 (pH adjusted to 7.4, 310 mOsm) or, for current-clamp (in mM) 130 $KMeSO_3$, 10 NaCl, 10 Hepes, 2 $MgCl_2$, 0.5 EGTA, 0.16 $CaCl_2$, 4 $Na_2ATP$, 0.4 NaGTP, and 14 Tris-creatine phosphate (pH adjusted with NaOH to 7.3, 310 mOsm). The bath solution contained (in mM) 140 NaCl, 5 KCl, 2 $CaCl_2$, 1 $MgCl_2$, 10 glucose, and 10 Hepes-NaOH (pH 7.4). An extracellular concentric bipolar electrode (FHC) was placed on the culture monolayer at a distance of approximately 80 μM from the recording cell, as previously described (32). Evoked responses were induced by injecting a 1-ms, 1-mA current through an Isolated Pulse Stimulator 2100 (A-M Systems) connected to the stimulating electrode. For voltage-clamp experiments, the holding potential was −70 mV, except for NMDAR-mediated EPSC recordings where the measurements were performed at +40 mV. The PPR for GABAR- and NMDAR-mediated evoked responses was measured with a 50-ms interval between successive stimulation pulses. The coefficient of variation for AMPAR-mediated evoked EPSCs was calculated (SD/mean) from 5–10 consecutive trials. The pharmacological agents were picrotoxin (50 μM; Tocris), 6-Cyano-7-nitroquinoxaline-2,3-3-dione (CNQX, 25 μM; Tocris), DL-2-Amino-5-phosphonopentanoic acid (DL-AP5, 50 μM; Tocris), TTX (a voltage-gated $Na^+$-channel blocker, 1 μM; Ascent Scientific), and tetraethylammonium and 4-aminopyridine (TEA and 4AP, voltage-gated $K^+$-channel blockers, 10 mM and 1 mM, respectively; Tocris). The AP-generation experiments on iN cells were performed at approximately −60 mV by using a small holding current to adjust the membrane potential accordingly. Puff application of 50 μM AMPA (R-S AMPA hydrobromide; Tocris) was performed for 100 ms using a Picospritzer III (Parker Instrumentation).

**Statistical Tests.** Cumulative plots were generated from parameters collected from individual cells under similar experimental conditions. Average data are presented as bar graphs indicating means ± SEM. The number of cells included for each analysis is presented in the corresponding bar graphs as total number of cells/number of independent cultures. Statistical comparisons between bar graphs were made using the unpaired, one-tail, Student *t* test (*$P < 0.05$, **$P < 0.01$, and ***$P < 0.001$, all versus control). Experiments were performed in a blinded fashion; i.e., the experimenter was unaware of the genotype of the samples being studied.

**ACKNOWLEDGMENTS.** We thank all members of the T.C.S. and M.W. laboratories for helpful discussions. This study was supported by National Institutes of Health Grants R01 MH092931 and AG010770-18A1 (to T.C.S. and M.W.), and a Dean's Postdoctoral Fellowship (to S.M.). M.W. is a New York Stem Cell Foundation-Robertson Investigator.

1. Takahashi K, Yamanaka S (2006) Induction of pluripotent stem cells from mouse embryonic and adult fibroblast cultures by defined factors. *Cell* 126(4):663–676.
2. Hanna JH, Saha K, Jaenisch R (2010) Pluripotency and cellular reprogramming: Facts, hypotheses, unresolved issues. *Cell* 143(4):508–525.
3. Watanabe A, Yamada Y, Yamanaka S (2013) Epigenetic regulation in pluripotent stem cells: A key to breaking the epigenetic barrier. *Philos Trans R Soc Lond B Biol Sci* 368(1609):20120292.
4. Ito D, Okano H, Suzuki N (2012) Accelerating progress in induced pluripotent stem cell research for neurological diseases. *Ann Neurol* 72(2):167–174.
5. Marchetto MC, Brennand KJ, Boyer LF, Gage FH (2011) Induced pluripotent stem cells (iPSCs) and neurological disease modeling: Progress and promises. *Hum Mol Genet* 20(R2):R109–R115.
6. Chambers SM, Studer L (2011) Cell fate plug and play: Direct reprogramming and induced pluripotency. *Cell* 145(6):827–830.
7. Han SS, Williams LA, Eggan KC (2011) Constructing and deconstructing stem cell models of neurological disease. *Neuron* 70(4):626–644.
8. Vierbuchen T, et al. (2010) Direct conversion of fibroblasts to functional neurons by defined factors. *Nature* 463(7284):1035–1041.
9. Pang ZP, et al. (2011) Induction of human neuronal cells by defined transcription factors. *Nature* 476(7359):220–223.
10. Pfisterer U, et al. (2011) Direct conversion of human fibroblasts to dopaminergic neurons. *Proc Natl Acad Sci USA* 108(25):10343–10348.
11. Caiazzo M, et al. (2011) Direct generation of functional dopaminergic neurons from mouse and human fibroblasts. *Nature* 476(7359):224–227.
12. Yoo AS, et al. (2011) MicroRNA-mediated conversion of human fibroblasts to neurons. *Nature* 476(7359):228–231.
13. Qiang L, et al. (2011) Directed conversion of Alzheimer's disease patient skin fibroblasts into functional neurons. *Cell* 146(3):359–371.
14. Ladewig J, et al. (2012) Small molecules enable highly efficient neuronal conversion of human fibroblasts. *Nat Methods* 9(6):575–578.
15. Yang N, Ng YH, Pang ZP, Südhof TC, Wernig M (2011) Induced neuronal cells: How to make and define a neuron. *Cell Stem Cell* 9(6):517–525.
16. Zhang Y, et al. (2013) Rapid single-step induction of functional neurons from human pluripotent stem cells. *Neuron* 78(5):785–798.
17. Marchetto MC, et al. (2010) A model for neural development and treatment of Rett syndrome using human induced pluripotent stem cells. *Cell* 143(4):527–539.
18. Brennand KJ, et al. (2011) Modelling schizophrenia using human induced pluripotent stem cells. *Nature* 473(7346):221–225.
19. Lee G, et al. (2009) Modelling pathogenesis and treatment of familial dysautonomia using patient-specific iPSCs. *Nature* 461(7262):402–406.
20. Paşca SP, et al. (2011) Using iPSC-derived neurons to uncover cellular phenotypes associated with Timothy syndrome. *Nat Med* 17(12):1657–1662.
21. Etherton MR, Tabuchi K, Sharma M, Ko J, Südhof TC (2011) An autism-associated point mutation in the neuroligin cytoplasmic tail selectively impairs AMPA receptor-mediated synaptic transmission in hippocampus. *EMBO J* 30(14):2908–2919.
22. Südhof TC (2008) Neuroligins and neurexins link synaptic function to cognitive disease. *Nature* 455(7215):903–911.
23. Song JY, Ichtchenko K, Südhof TC, Brose N (1999) Neuroligin 1 is a postsynaptic cell-adhesion molecule of excitatory synapses. *Proc Natl Acad Sci USA* 96(3):1100–1105.
24. Varoqueaux F, Jamain S, Brose N (2004) Neuroligin 2 is exclusively localized to inhibitory synapses. *Eur J Cell Biol* 83(9):449–456.
25. Ichtchenko K, Nguyen T, Südhof TC (1996) Structures, alternative splicing, and neurexin binding of multiple neuroligins. *J Biol Chem* 271(5):2676–2682.
26. Irie M, et al. (1997) Binding of neuroligins to PSD-95. *Science* 277(5331):1511–1515.
27. Jamain S, et al.; Paris Autism Research International Sibpair Study (2003) Mutations of the X-linked genes encoding neuroligins NLGN3 and NLGN4 are associated with autism. *Nat Genet* 34(1):27–29.
28. Tabuchi K, et al. (2007) A neuroligin-3 mutation implicated in autism increases inhibitory synaptic transmission in mice. *Science* 318(5847):71–76.
29. Etherton M, et al. (2011) Autism-linked neuroligin-3 R451C mutation differentially alters hippocampal and cortical synaptic function. *Proc Natl Acad Sci USA* 108(33):13764–13769.
30. Tucker KL, Meyer M, Barde YA (2001) Neurotrophins are required for nerve growth during development. *Nat Neurosci* 4(1):29–37.
31. Saha K, Jaenisch R (2009) Technical challenges in using human induced pluripotent stem cells to model disease. *Cell Stem Cell* 5(6):584–595.
32. Maximov A, Pang ZP, Tervo DG, Südhof TC (2007) Monitoring synaptic transmission in primary neuronal cultures using local extracellular stimulation. *J Neurosci Methods* 161(1):75–87.
33. Cao P, Maximov A, Südhof TC (2011) Activity-dependent IGF-1 exocytosis is controlled by the $Ca^{(2+)}$-sensor synaptotagmin-10. *Cell* 145(2):300–311.